JOURNAL OF GEOPHYSICAL RESEARCH, VOL. 95, NO. A8, PAGES 12,277–12,286, AUGUST 1, 1990

A Wave-Particle-Wave Interaction Mechanism as a Cause of VLF Triggered Emissions

L. A. D. SÁ

Space, Telecommunications and Radioscience Laboratory, Stanford University, Stanford, California

A narrowband-filter spectral analysis is made of VLF emissions triggered by discrete waves transmitted from Siple Station, Antarctica and received at Lake Mistissini, Quebec, after ducted mode propagation. It is found that triggered emissions have a spectral structure similar to magnetospheric sidebands. As in the case of regular sidebands, their spectra and evolution are affected by the presence of power line radiation (PLR). Triggered emissions associated with monochromatic wave transmissions are explained as being caused by the interaction of the incoming wave with PLR. The issue of the importance of extremely weak signals in these phenomena is addressed, and it is shown that when a wave is perturbed by a weaker signal, sidebands and, consequently, triggered emissions can occur even if the amplitude ratio of the two signals is -50 dB. For such cases, the two waves should not be separated by a frequency larger than a few times the stronger wave trapping frequency. A mechanism, based on previous theoretical work, is presented to explain the creation and evolution of the triggered emissions studied in the paper.

1. Introduction

Many papers have been written in the past on the subject of VLF emissions triggered in the Earth's magnetosphere. Many models were also presented in an effort to explain their creation and evolution. All such models assumed that triggered emissions were created from a single monochromatic wave interacting with the magnetospheric plasma [e.g., *Nunn*, 1989; *Molvig et al.*, 1988; *Carlson*, 1987; *Helliwell and Inan*, 1982; *Dowden et al.*, 1978; *Nunn*, 1974; *Helliwell and Crystal*, 1973; *Dysthe*, 1971; *Das*, 1968]. (*Paschal and Helliwell* [1984] provide a careful description of some of those papers.) This paper follows a different route: Instead of abstracting the triggering process and trying to reproduce it by means of computer simulations, we carefully analyze the experimental spectra, recorded on digital tape, with the help of narrow bandwidth filters (1.56 Hz), and note their most significant characteristics. As suggested by *Sá and Helliwell* [1988], we find that, analogously to magnetospheric sidebands, triggered emissions are a multiwave effect, their spectral structure being similar to the sideband spectral structure. Triggered emissions created by single-frequency transmissions are formed by the interaction of that single wave with power line radiation (PLR) assumed to be present in the duct. Triggered emissions associated with double-frequency transmissions are created by the combined effects of the transmitted waves and PLR, their frequency spectra showing evidence of the importance of them both. The theoretical framework capable of explaining the wave-particle-wave interactions responsible for such observed effects was developed by *Sá* [1989*a*, *b*, *c*]. (This three-part paper will be referred to as I, II, and III, from here on.)

Since the importance of extremely weak waves in sideband and triggered emission formation seems to be a remarkable and consistent property of the magnetospheric plasma, some consideration must be given to it. *Sá and Helliwell* [1988] already gave experimental evidence that an amplitude ratio of -40 dB between a wave and a perturbing companion is not enough to eliminate the perturbation effects. In III, some theoretical evidence supporting this result was also given, but the point was not systematically approached. Section 2 of this paper makes a theoretical analysis of the wave-particle-wave interaction process, concluding that sizable effects can be created by wave perturbations having an amplitude ratio of -50 dB with respect to the main wave. Section 3 gives an overall description of the data analyzed, and section 4 goes over the data in detail, showing that several theoretical and observational assumptions about triggered emissions are indeed supported by the data. Section 5 gives a theoretical description of the proposed fundamental process for the creation of triggered emissions; triggered emissions are shown to be caused by a wave-particle-wave interaction capable of producing resonances and chaos in the electron motion of the magnetospheric plasma. Section 6 contains final discussions and conclusions.

Paper number 90JA01011.
0148-0227/90/90JA-01011$02.00

2. The Problem of Small Wave Intensities

Since both sideband formation and the triggered emission data presented in this paper indicate experimentally the importance of weak waves in the evolution of the observed electromagnetic spectra, a theoretical analysis is made in this section of the importance of such weak perturbations on stronger waves propagating in the magnetospheric plasma. For such a study we use phase plots, computed numerically using the method of the Poincaré surfaces of section, where the presence of waves is indicated by the formation of resonances. A detailed explanation of such phase plots, their interpretation, and the equations describing the electron motion from which they are derived, are found in I and II. The same reference also contains a general exposition of the wave-particle-wave process responsible for the occurrence of sidebands and triggered emissions, and defines the notation used in this section.

In the absence of wave-wave interactions, the electrons should move under the linearly added effects of each wave in the plasma, and the phase plots should contain only the isolated resonances associated with each incoming wave. If ad-

ditional resonances appear we must conclude that the waves are interacting and that those new resonances, analogously to the carrier resonances, should produce discrete waves. That this is indeed the case is shown in I and II. In this paper, we use the phase plots as a laboratory for the detection of wave-wave interactions. We perturb a stronger wave with a weaker one of variable amplitude, and check for the presence of resonances. If resonances of appreciable size are formed, we conclude that the weak wave is capable of affecting the radiation spectra in a measurable way.

Figure 1 shows the result of such calculations. Each of the three phase plots describes the effect of adding to the electromagnetic spectrum, initially defined by a single wave

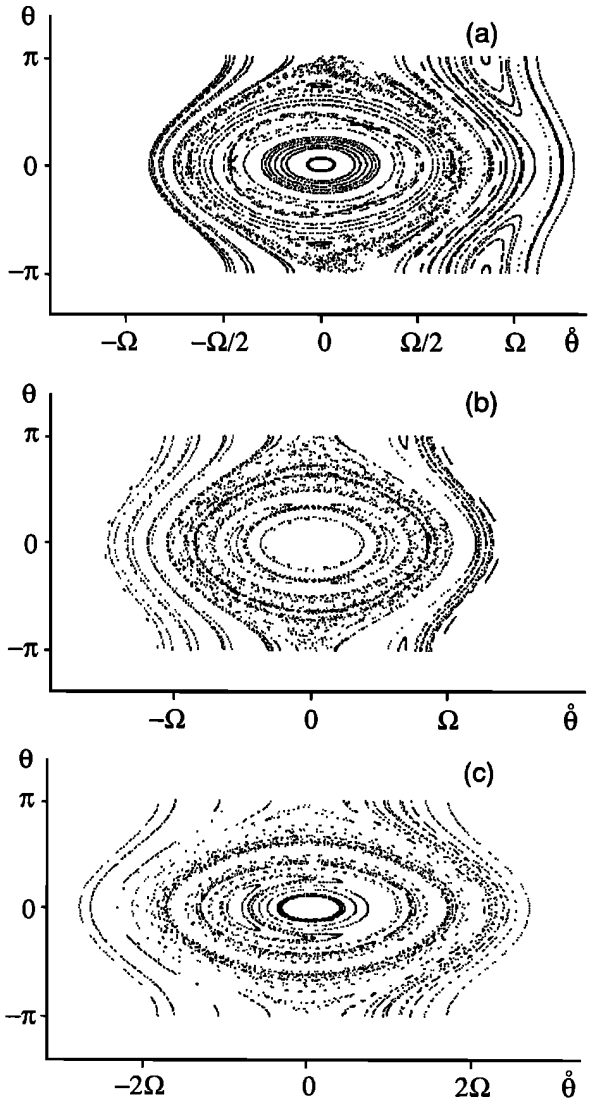

Fig. 1. Effect of weak monochromatic perturbations on electromagnetic spectra. The perturbing wave is located at a frequency Ω above the stronger carrier and its phase is shifted by 180° relatively to the main carrier phase. The angle θ measures the electron position relative to the main wave electromagnetic field. The presence of an interaction is indicated by the presence of resonances "trapped" inside the main wave resonance: (*a*) α = -30 dB. A three-lobed resonance, that will radiate at the frequencies Ω, $2\Omega/3$, and $\Omega/3$ is seen. (*b*) α = -45 dB. A two-lobed resonance, that will radiate at the frequencies Ω and $\Omega/2$ is created. (*c*) α = -50 dB. A single-lobed resonance, that will radiate at the frequency Ω is seen.

at $\theta = 0$, another one at $\dot{\theta} = \Omega$. θ measures the electron position relative to the main wave electromagnetic field. α is the ratio of the weak to strong wave amplitudes.

For a given value of α, each of the phase plots depends only on the ratio Ω/Ω_t. The strong-wave trapping frequency, Ω_t, is a free parameter, being allowed to take values both above and below trapping levels. Higher values of Ω_t in the same plot imply larger values of the wave-wave frequency separation, Ω. For a given value of Ω_t, each plot is valid for a whole range of pitch angles: large pitch angles and small wave amplitudes produce the same effect as small pitch angles and large wave amplitudes.

The trapping threshold is not directly relevant to the results obtained because, as discussed in I and II, the relevant objects are resonances and not individual electrons. Radiation is produced by the oscillation of resonances inside the stronger carrier potential well. They can occur whether the electron is able to execute full oscillations in the potential well or not.

In Figure 1*a*, α = -30 dB and $\Omega/\Omega_t = 3$. We see that within the resonance area corresponding to the main carrier another resonance is formed. It consists of a three-island chain with an area comparable to that of the larger resonance. (The islands are centered at $(\theta, \dot{\theta}) \approx (\pm\pi/3, -\Omega/4)$ and $(0, \Omega/2)$.) Such a resonance will radiate mostly at the 1/3-subharmonic and 1st harmonic frequencies of the two-wave frequency separation.

Figure 1*b* shows the consequence of making the perturbation even weaker. α is now -45 dB and the frequency separation has been slightly decreased to compensate for the lower perturbation amplitude ($\Omega/\Omega_t = 2$). A two-island chain is seen. (The islands are centered at $(\theta, \dot{\theta}) \approx (0, \pm\Omega/2)$.) It will radiate at the 1/2-subharmonic and 1st harmonic frequencies.

Figure 1*c* shows an extreme case in which α = -50 dB. The frequency separation between the two waves is now equal to the trapping frequency of the strong wave ($\Omega/\Omega_t = 1$). The resonance of the weak wave is not allowed to form because of the presence of the stronger resonance. A resonance due to the two-wave interaction, centered approximately at $(0, -\Omega)$, is seen indicating that even at those extremes, a sizable wave-wave interaction is still possible. Radiation will be created at the 1st harmonic frequency. That this last case is the most efficient for the creation of perturbation effects, has already been realized by several other authors [*Dowden*, 1982; *Serra*, 1984; *Nunn*, 1986].

Those pictures indicate what was already established experimentally: the simple fact that a signal is not strong enough to be directly detectable is no reason to eliminate the possibility that, through its interaction with stronger signals, it may produce easily detectable effects that may play a fundamental role in spectra formation. The data in this paper show that triggered emissions consist of time-dependent sidebands, sometimes formed only by the interaction of a single incoming wave with power line harmonic (PLH) radiation. We arrive then at the conclusion that despite its weakness, PLR may be fundamental for the creation and evolution of triggered emissions in the magnetosphere.

3. General Properties of the Data

The data analyzed and shown in Figures 2–5 and 6–9, are part of a larger set of about 40 pulses, many of them giving rise to several triggered emissions. The set was chosen for the strength of the received signal combined with weak

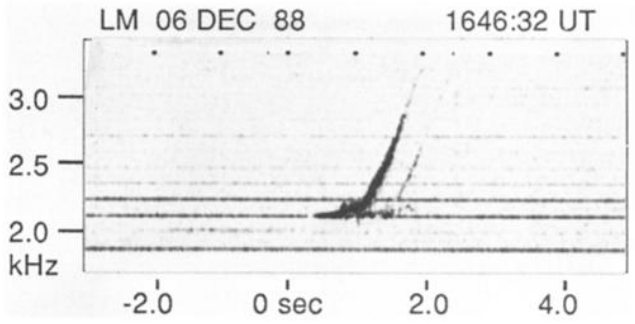

Fig. 2. Emission triggered at the beginning of a single-frequency one-second pulse transmitted at a PLH frequency (2100 Hz). 10 Hz bandwidth filters were used. The same spectrum is analyzed with fine filters in Figure 6.

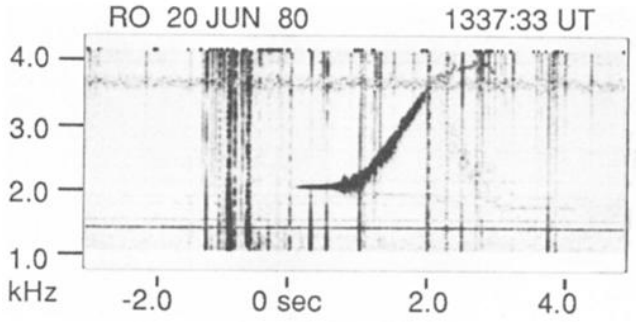

Fig. 4. Emission triggered at the end of a one-second single-frequency pulse transmitted 20 Hz above a PLH frequency (2000 Hz). 10 Hz bandwidth filters were used. The same spectrum is analyzed with fine filters in Figure 8.

background noise, and the absence of appreciable multipath effects. From the whole set, three representative examples were selected based on the fact that the displayed triggered emission was either isolated or fairly separated from others preceding or following it. Additionally, the condition was imposed that no strong spherics should affect the pulse transmissions, and that the measured spectra should not be extremely complicated. The data were obtained from digital recordings made at an amplitude low enough so as to avoid signal overloading, even when spherics were present. The pulse represented in Figures 4 and 8 is a special case. It is a single frequency one second pulse coming from an older analog recording, its importance being mostly historical: it was analyzed by *Paschal and Helliwell* [1984], and was used as a model for simulation programs by *Carlson* [1987]. It is the only example presented of termination triggering (i.e., triggering at the end of a transmitted pulse). Figures 2 and 6 show a case of a single-frequency transmission triggering a single pre-termination emission. Figures 3 and 7, 5 and 9, are double-frequency transmissions, also producing pre-termination triggerings.

Figures 2–5 show the triggered emissions as they look when displayed with spectral ranges of 1.5 kHz and 3.0 kHz obtained with 10 Hz filters. Figures 6*a*–9*a* show the spectra as they look when a fine filter (1.56 Hz) analysis is made and the results are displayed within a bandwidth of approximately 170 Hz. The main features, found in all of the fine-filter spectra (Figures 6*a*–9*a*), are that the transmitted waves grow, shift in frequency, create sidebands and collapse. The created sidebands linger on and produce more upper-frequency sidebands. The low-frequency ones die out, resulting in an upward moving spectrum that is observed as a standard triggered emission when analyzed with wider filters (Figures 2–5).

No cases have been found in which this sideband structure is not present. However, since the amount of data we present is limited, one should not conclude on experimental grounds alone that all possible triggered emissions consist of layered sidebands.

If the description we made is really correct the observed sidebands should be at the frequencies predicted by the KAM theorem (see I or II),

$$\omega = \frac{\sum_{i=1}^{N} n_i \omega_i}{\sum_{i=1}^{N} n_i} \tag{1}$$

as required by the equations of motion (in the above equation, n_i are arbitrary integers, ω_i are frequencies of waves present in the spectra, and ω is the possible frequency of a newly created sideband wave). A reason must also exist for the collapse of the low-frequency sidebands combined with the growth of the upper-frequency ones. Those two points are discussed in sections 4 and 5.

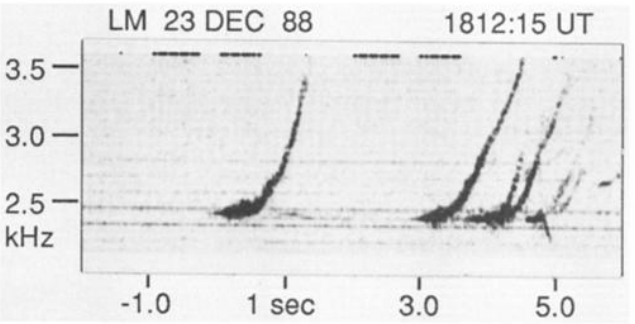

Fig. 3. Emissions triggered by two single-frequency carriers separated by 25 Hz. The lower carrier is transmitted at a PLH frequency (2340 Hz). 10 Hz bandwidth filters were used. After the first second, the upper carrier has its transmitted amplitude linearly decreased at the rate of -10 dB/s. The first emission in the sequence, occurring when the two transmitted amplitudes are the same, is analyzed with fine filters in Figure 7.

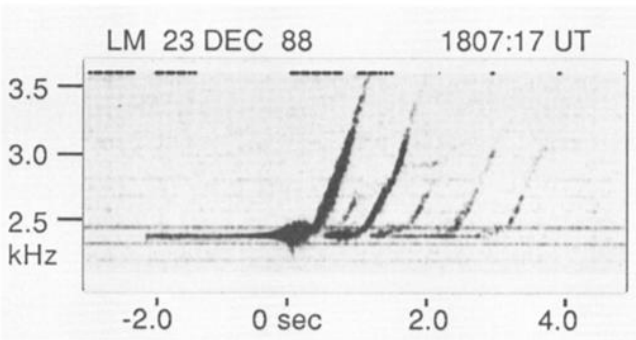

Fig. 5. Emissions triggered by two single-frequency carriers separated by 20 Hz. The upper carrier is transmitted at a PLH frequency (2340 Hz). 10 Hz bandwidth filters were used. After the first second, the lower carrier has its transmitted amplitude linearly decreased at the rate of -10 dB/s. The first emission in the sequence is analyzed with fine filters in Figure 9.

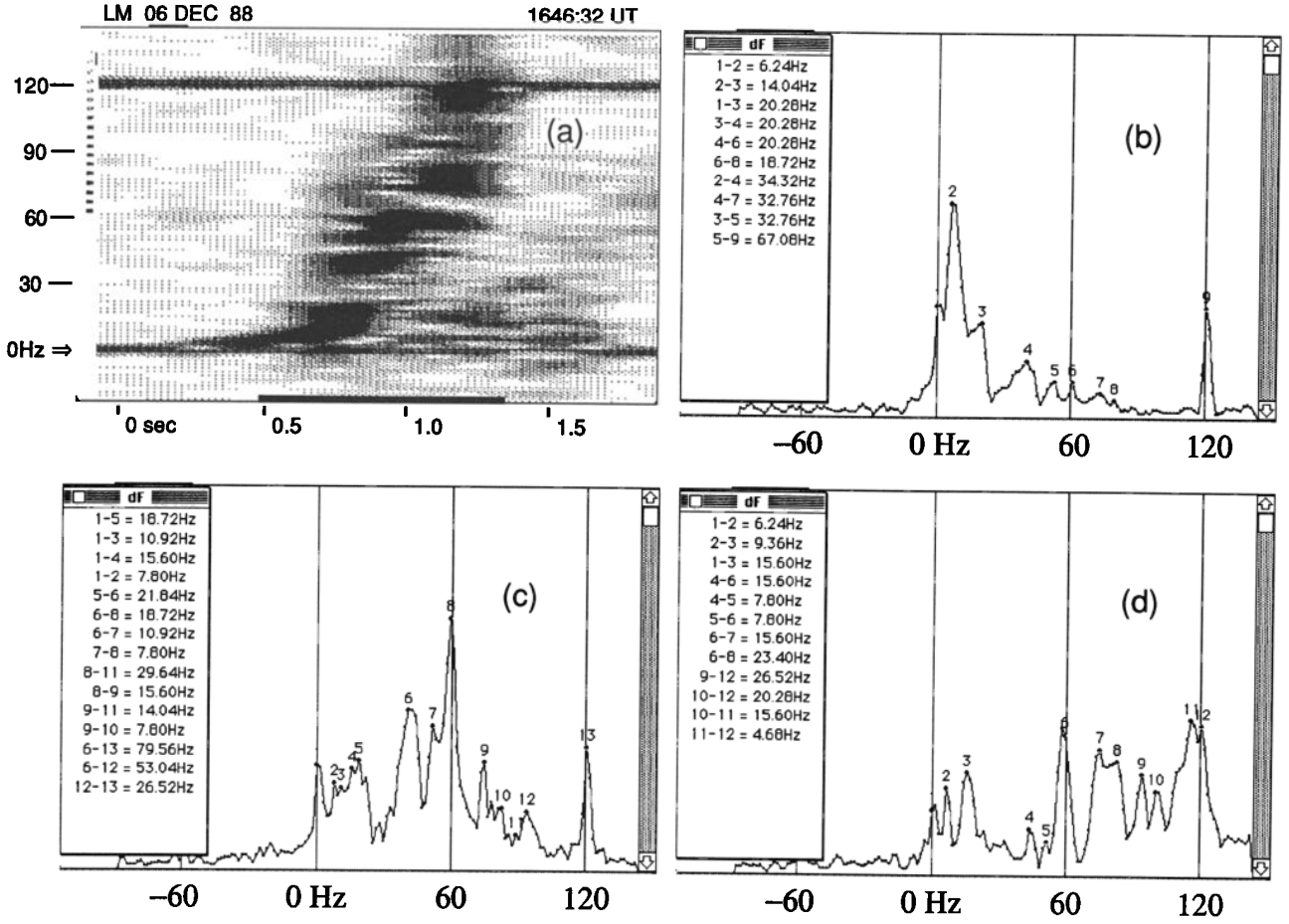

Fig. 6. Triggered emission caused by a single constant frequency carrier: (*a*) Time dependent spectrum of the electromagnetic field. 1.56 Hz bandwidth filters were used. The arrow shows the carrier transmission frequency. 0 Hz in the vertical coordinate axis corresponds to 2100 Hz. The time interval marked by a horizontal bar at the bottom is divided into three equal parts and the spectrum averaged over each of them. (*b*)–(*d*) Successive averages of the spectrum shown in Figure 6*a*. The windows at the left of each averaged spectrum contain a table of frequency differences: at the left of each equal sign are two digits representing two spectral lines; at the right is their frequency difference. The vertical scale is linear, arbitrary, and the same for all three spectra.

4. Detailed Analysis of Spectral Structures

Single-Frequency Pre-Termination Triggering

The first emission, shown in Figures 2 and 6, is triggered by a one second, constant frequency and constant amplitude pulse transmitted at a PLH frequency (2100 Hz). Figure 6*a* shows the time dependent spectrum obtained with the use of 1.56 Hz filters. The two strong lines crossing the spectrum at 0 Hz and 120 Hz (relative frequencies) are local induction lines and are not directly relevant to the spectrum. The horizontal black line at the bottom of Figure 6*a* is the time interval over which the transmission was analyzed. This interval was divided into three equal parts and the average spectra obtained are shown, ordered in time, in Figures 6*b* to 6*d*.

Figure 6*b* shows the beginning of the triggered emission and is virtually indistinguishable from sideband spectra such as the ones shown in *Sá and Helliwell* [1988]. The main wave, initially transmitted at 0 Hz, has grown, shifted in frequency, and excited sidebands by interacting with the adjacent PLHs. The main excitation is of 1/3 subharmonics of 60 Hz, separated by 20 Hz from each other. Those are lines 3 and 4. Lines 3 and 4 in turn create two harmonics of 20 Hz, lines 6 and 8. Additionally, since 4 has an appreciable amplitude, it interacts with 2 to create a first harmonic, line 7. Line 5 is a subharmonic of line 3 and the PLH present at 120 Hz. It is a 1/3 subharmonic that should ideally be located 33.3 Hz above line 3 and 66.7 Hz below line 9. The measured frequency differences are 32.76 and 67.08 Hz. Since lines 1 and 9 are mostly induction lines, their heights do not represent the amplitude values of the PLH located at those frequencies.

The transition from Figure 6*b* to Figure 6*c* is theoretically explained in section 5. In brief, the upper frequency sidebands destroy the resonance that produces growth of the transmitted carrier. The carrier collapses, releasing the electrons it had bunched. Such electrons move upwards in frequency, due to the inhomogeneity of the Earth's magnetic field, and feed the upper sideband growth.

Figure 6*c* shows the collapsed transmitted carrier, the transfer of energy upwards in frequency, the growth of sidebands formed in Figure 6*b*, and the beginning of the next cycle of sideband formation. Lines 6, 7, and 8 in Figure 6*c*

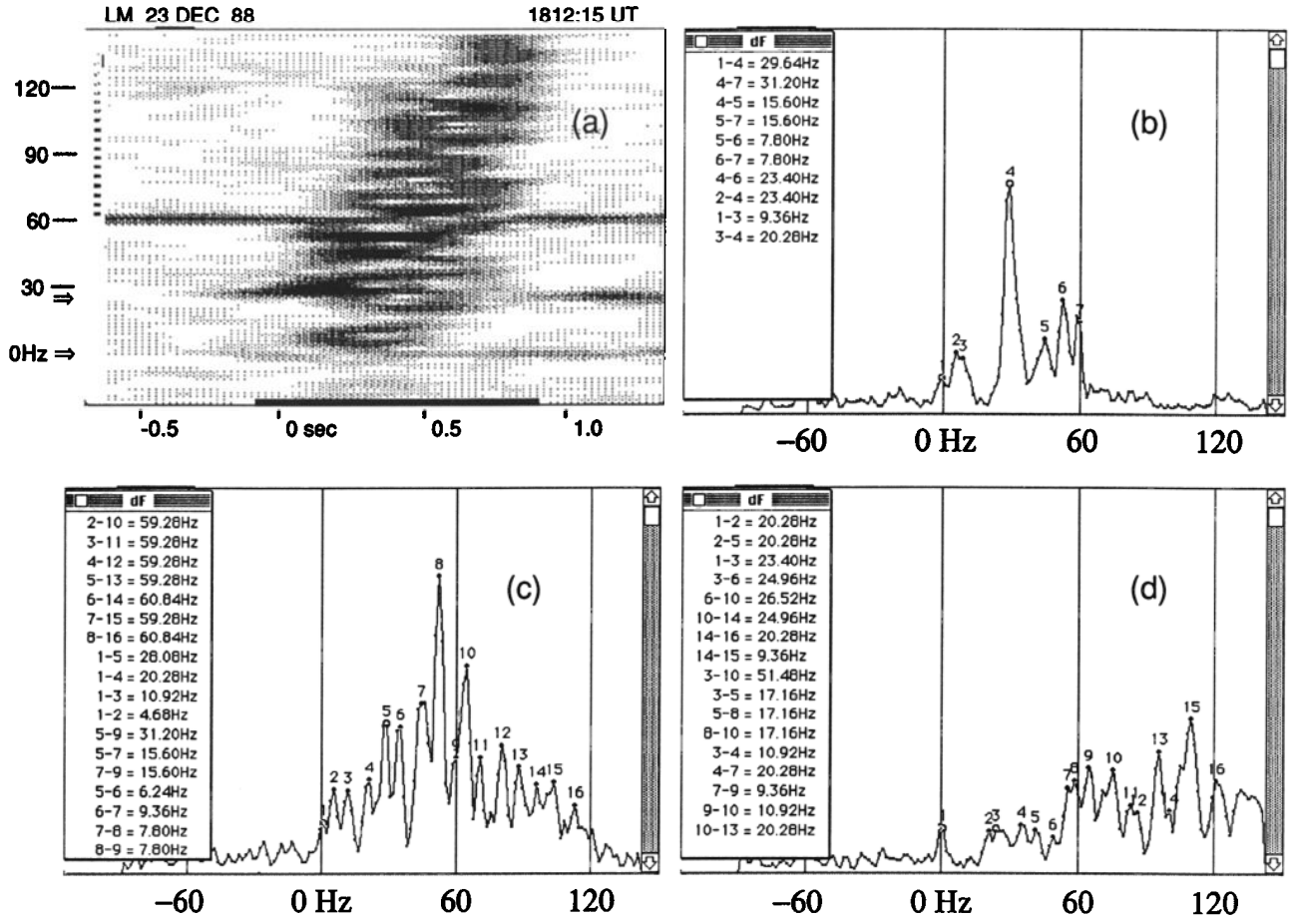

Fig. 7. Triggered emission caused by two constant-frequency equal-amplitude carriers. The conventions used are the same as in Figure 6: (*a*) The arrows show the transmission frequency of each carrier. They are separated by 25 Hz. 0 Hz in the vertical coordinate axis corresponds to 2340 Hz. (*b*)–(*d*) Successive averages of the spectrum shown in Figure 7*a*.

correspond to lines 4, 5, and 6 in Figure 6*b*. They have undergone a large amount of growth. Line 8 has the highest amplitude and lasts the longest. Such a concentration of electromagnetic energy at a fixed frequency is called an entrainment of the triggered emission, in this case by a PLH. Such an entrainment can be observed fairly clearly in Figure 6*a*. The fine structure found on the collapsed transmitted carrier is a collection of 60 Hz subharmonics: Lines 4 and 5 are nominally 1/4 and 1/3 subharmonics of lines 1 and 8. (This is true within one filter bandwidth.) Lines 2 and 3 are 1/2 subharmonics of lines 1 and 4, and 1 and 5. Lines to the right of line 8 can be explained by successive bifurcations of the interval defined by lines 8 and 13. A first division by two creates line 11. The interaction of lines 8 and 11 creates line 9, halfway between them. Lines 9 and 11 create line 10, another 1/2 subharmonic. Additional subdivisions can be seen but have not been recorded in the frequency difference table at the left. Line 12 is more complicated: it starts as a 1/2 subharmonic of 9 and 13. As line 6 grows, line 12 shifts so that it becomes a 1/3 subharmonic of line 6 and 13.

The transition from Figure 6*c* to 6*d* is explained by the same mechanism as before: the sidebands located on the upper side of line 8 in Figure 6*c* grow, destroying the resonances associated with the stronger waves (6, 7, and 8). The stronger waves collapse, release electrons, and the triggered emission moves upward in frequency.

Figure 6*d* shows collapsed waves in the interval 0 Hz to 60 Hz, most of the radiation being located between 60 Hz and 120 Hz. Lines 7 , 8, and 9 in Figure 6*d* are amplifications of lines 9, 10, and 12 in Figure 6*c*. Lines 10 and 11 are the two remaining lines of a subdivision process that split the interval defined by lines 9 and 12 into 5 equal parts. The resulting set of four waves, separated by 5 Hz intervals, would be seen if an observation were made of each spectral slice that composes the average shown in Figure 6*d*. The averaging process eliminated the two waves central to the subdivided interval, only a hump being still visible. In the 0 Hz to 60 Hz interval, lines 2 and 3 are the remainders of 2 and 4 in Figure 6*c*. Line 5 is the 1/2 subharmonic of 4 and 6. Line 4 is a first harmonic of 6 and 7.

Equal-Amplitude Double-Frequency Pre-Termination Triggering

Figures 3 and 7*a* show a triggered emission created by a two-frequency pulse. The two waves have the same transmitted amplitude and the triggering coincides with the start of the transmission. The constant amplitude line at 60 Hz

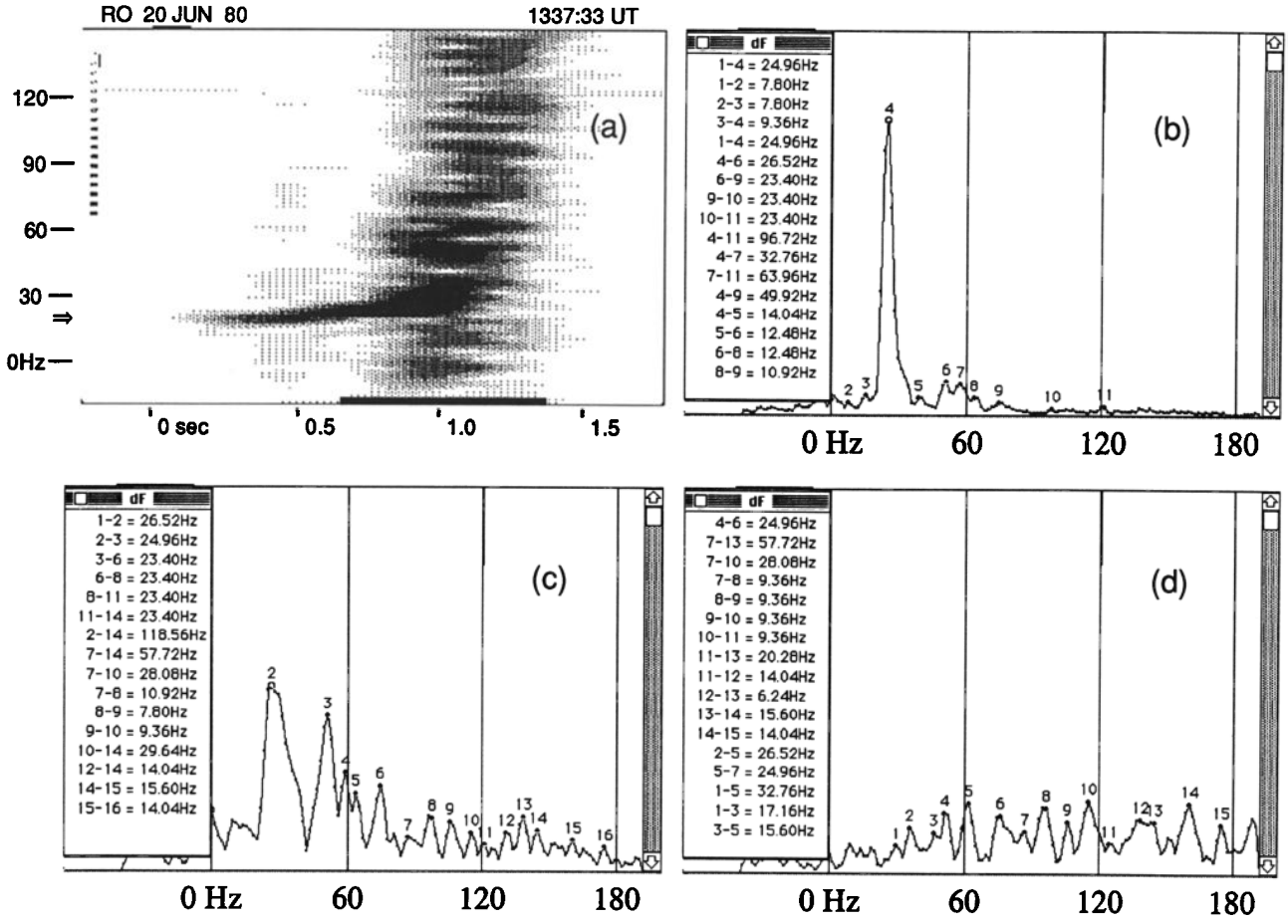

Fig. 8. Triggered emission caused by a single constant-frequency carrier. The conventions used are the same as in Figure 6: (*a*) The arrow shows the carrier transmission frequency. 0 Hz in the vertical coordinate axis corresponds to 1980 Hz. (*b*)–(*d*) Successive averages of the spectrum shown in Figure 8*a*.

is an induction line. The two waves are separated by 25 Hz, and the lower frequency one is transmitted at a PLH frequency (2340 Hz).

Figure 7*b* shows the first part of the spectrum, which again is identical to the ones obtained from normal sideband formation. It is seen that the lower frequency wave has not grown much, its peak (line 1) being fairly close to the noise level. The upper frequency carrier, on the other hand is by far the strongest wave in the spectrum. Its frequency is changed by 5 Hz, so that now it is located halfway between the two PLHs at 0 Hz and 60 Hz. The strong wave (line 4) interacts with the PLH located at the position of line 7 (which is mostly an induction line), creating line 5 (a 1/2 subharmonic). Line 5 interacts with the same PLH to create line 6 (another 1/2 subharmonic). Lines 4 and 6 interact to create line 2, a first harmonic. Line 3 is a 1/3 subharmonic of lines 1 and 4.

The transition from Figure 7*b* to Figure 7*c* is explained by the destruction of the resonance associated with line 4, and subsequent growth of the upper frequency subharmonics. This time however, the collapse is not as complete and as fast as in the example of the previous subsection. In Figure 7*c* the main carrier is represented by line 5 which is approximately, but not exactly, 30 Hz above line 1, something that should be expected, since the collapse of an amplified wave has the tendency to shift it back to the original transmission frequency. This spectrum has a remarkable property that we highlight by changing the method used to identify each wave. If we look at the frequency difference table at the left of the picture, we see that each line in the 60 Hz to 120 Hz interval (lines 10 to 16) can be obtained from each line in the 0 Hz to 60 Hz interval (lines 2 to 8) by a 60 Hz displacement. Since the transmitted frequency difference was 25 Hz, this fact is remarkable, indicating that 60 Hz is indeed one of the frequencies present in the magnetospheric plasma, and should be partly responsible for the structure of the spectra there observed. The formation of lines 2 to 6 can be understood as a frequency interval subdivision process: lines 3 and 4 are the 1/3 subharmonics of the interval defined by 1 and 5. Line 2 bifurcates the interval defined by lines 1 and 3. Line 7 is the 1/2 subharmonic of 5 and the PLH at position 9. Lines 6 and 8 are 1/2 subharmonics of lines 5 and 7, and 7 and 9.

Figure 7*d* shows the spectrum after sideband growth coupled with stronger-wave resonance destruction has again occurred. The spectrum appears essentially meaningless, partly because now there are no stronger lines suggesting a starting point from which measurements should be made. An analysis starting from known transmitted frequencies can, however, shed some light on its structure: Lines 2 and

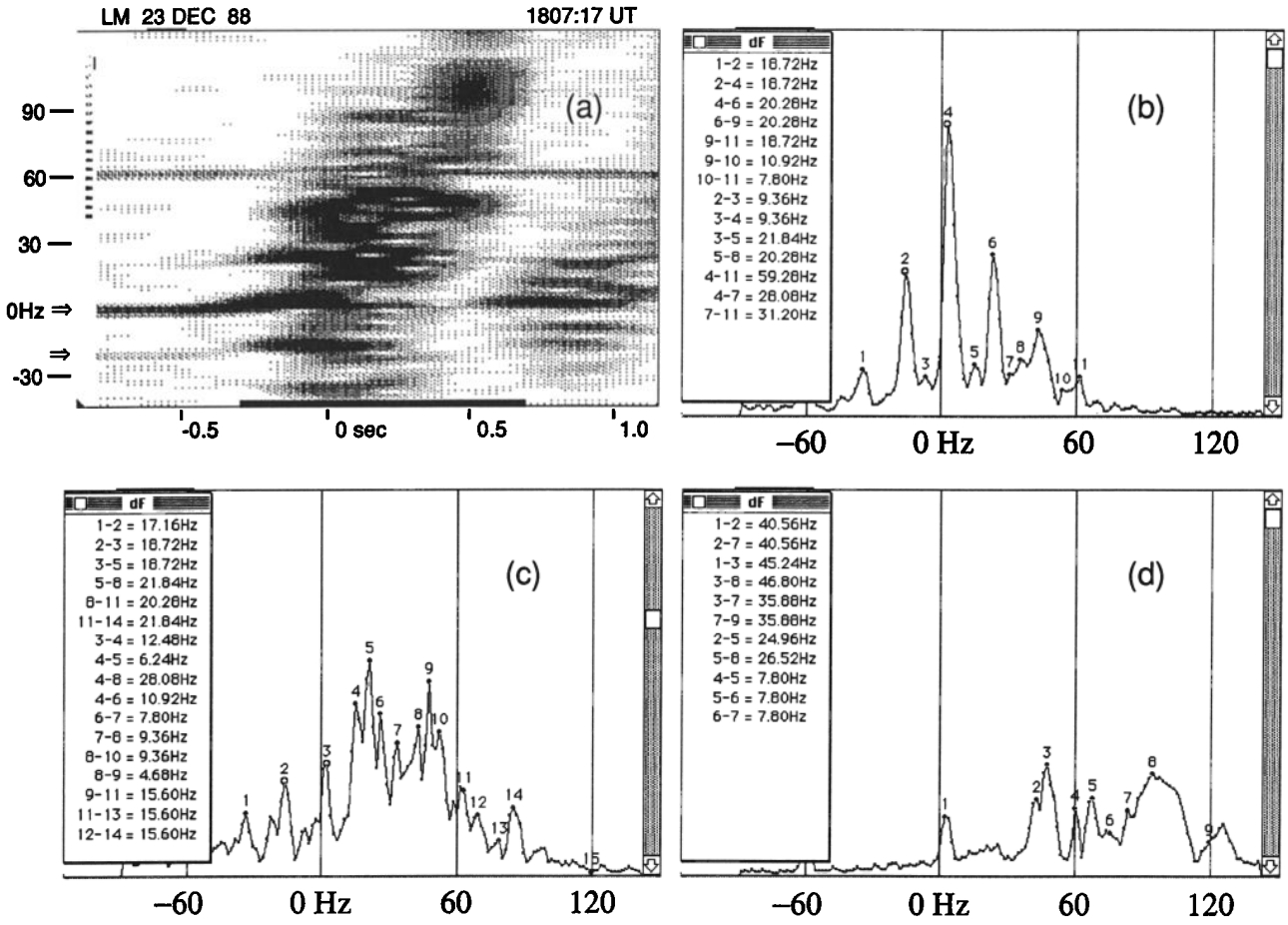

Fig. 9. Triggered emission caused by two constant-frequency variable-amplitude carriers. The conventions used are the same as in Figure 6: (*a*) The arrows show the transmission frequency of each carrier. They are separated by 20 Hz. 0 Hz in the vertical coordinate axis corresponds to 2340 Hz. The low-frequency carrier has a lower and linearly decreasing amplitude (-10 dB/s). At the moment of the triggered emission the amplitude ratio is -10 dB. (*b*)–(*d*) Successive averages of the spectrum shown in Figure 9*a*.

5, for instance, are the 1/3 subharmonics of the PLHs located at 0 Hz and 60 Hz. Lines 1 and 3 are the transmitted carriers separated nominally by 25 Hz. They create a series of 1st harmonics. Those are lines 3, 6, 10, and 14. The interaction of 14 and 16 creates their 1/2 subharmonic, line 15. The interaction of lines 3 and 10 creates their two 1/3 subharmonics, lines 5 and 8. Lines 6 in Figure 7*c* and line 4 in Figure 7*d* are the same. The interaction of 4 with 13 creates 9, that is their 1/2 subharmonic, and also 7 and 10, their 1/3 subharmonics. Additional weaker lines are seen, but we choose not to measure or analyze them.

Single-Frequency Termination Triggering

Figures 4 and 8*a* show a triggered emission at the end of a one second, constant frequency, constant amplitude pulse, transmitted 20 Hz above a PLH frequency (2000 Hz). As in the other cases, we see wave growth and frequency shift, followed by a burst of sidebands that essentially constitute the triggered emission. These data were recorded on analog tape, and do not have, in principle, the same quality as the other examples presented in this paper.

Figure 8*b* shows the amplified carrier, its shifted position, and the initial formation of upper frequency sidebands. The frequency shift is not arbitrary; in such cases the wave generally grows and shifts until its position is such as to divide an interval defined by two PLHs into an integral number of equal parts. In this case, the interval is the one defined by the PLHs located at 0 Hz and 120 Hz, and the number of parts is 5. This will define a frequency separation of 24 Hz. A more acurate analysis shows that in fact line 4, the carrier, shifts until it is approximately 25 Hz above the PLH, and interacts with it, creating a 1st harmonic, line 6. The interval between 6 and 11 is now divided into three equal parts, defining lines 9, 10 and 11. Line 7 is a 1/3 subharmonic of 4 and 11. Lines 5, 6, and 8 are 1/4 subharmonics of lines 4 and 9 (within one filter bandwidth). Lines 2 and 3 are 1/3 subharmonics of 1 and 4.

Figure 8*c* shows the spectrum when the upper frequency sidebands have grown appreciably and the transmitted carrier is beginning to collapse. Lines 3, 6, 8, 11, and 14 are separated approximately by 24 Hz, being the result of subdividing a 120 Hz interval into 5 equal parts. All other lines in the spectrum are obtained by a similar subdivision process so commonly responsible for the observed values of sideband frequencies: The basic interval to be divided is defined by lines 2 and 14, approximately 120 Hz apart. Line 7 is the 1/2 subharmonic of such an interval. Line 10 is the 1/2 subhar-

monic of 7 and 14. Lines 8 and 9 are the 1/3 subharmonics of 7 and 10. Line 12 is the 1/2 subharmonic of 10 and 14. Lines 15 and 16 are harmonics of the interval defined by 12 and 14. Additional lines can be seen and are easily shown to be 1/2 and 1/3 subharmonics of the above analyzed lines.

Figure 8*d* shows the tail end of the triggered emission. It is still organized, as most of its lines are the same as the ones present in Figure 8*c*. However, because all lines have approximately the same amplitude, such an organization is difficult to see. This type of spectrum is similar in appearance to the ones obtained from natural phenomena, indicating that natural radiation spectra may be organized (since the same laws of physics apply to them), but that the organization present in them may be nearly impossible to display convincingly. We leave to the reader the task of identifying the organization of Figure 8*d* by comparing it to Figure 8*c*, and using the table of frequency differences at the left of each picture.

Unequal-Amplitude Double-Frequency Pre-Termination Triggering

Figure 9*a* displays a triggered emission created by two constant frequency carriers separated by 20 Hz. This emission is the first one of the sequence shown in Figure 5. The upper frequency carrier is transmitted on a PLH frequency (2340 Hz) and has constant transmitted amplitude. The lower frequency carrier is having its transmitted amplitude linearly decreased at the rate of -10 dB/s. At the moment the triggered emission occurs, the transmitted lower carrier is 10 dB lower in amplitude than the upper frequency carrier.

Figure 9*b* shows the beginning of the triggering process. Lines 2 and 4 are the amplified and shifted carriers. At this point, sideband formation is already appreciable, and the carriers are at the beginning of the collapse process. Lines 1, 2, 6, 9, and 11 are harmonics of 2 and 4. Some frequency distortion is observed due to the different amounts of growth the two different carriers have undergone. Lines 3, 5, 8, and 10 are 1/2 subharmonics of such lines. Line 7 is the 1/2 subharmonic of 4 and 11. A concentration of radiation in the neighborhood of line 9 is already seen due, from the point of view described in this paper, to the electrons being ejected from the collapsing large carriers.

Figure 9*c* shows the collapsed carriers, lines 2 and 3, the motion of the radiation towards the upper frequency side, the formation of new sidebands in the 60 Hz to 120 Hz interval, and a complicated line structure clustering around the positions where lines 6 and 9 of Figure 9*b* were located. The harmonics of 2 and 3 are now lines 1, 5, 8, 11 and 14. All other lines are obtained by a subharmonic formation process: line 4 is a 1/3 subharmonic of 3 and 5, lines 6 and 7 are the 1/3 subharmonics of 4 and 8, line 10 is a first harmonic of 7 and 8, and line 9 is the 1/2 subharmonic of 8 and 10. Line 13 is the first harmonic of 9 and 11, and 12 is the mirror image of line 13 in the interval defined by 11 and 14 [*Sá and Helliwell*, 1988].

Figure 9*d* shows the spectrum almost completely collapsed in the interval where the triggered emission originated. Line 1 is the upper frequency carrier. (The lower frequency carrier has too low an amplitude to be seen.) Lines 2 and 7 are the 1/3 subharmonics of the interval defined by line 1 and the PLH at 120 Hz. Line 3 is a leftover from line 9 of Figure 9*c*. Its interaction with line 1 (the upper carrier) defines a first harmonic frequency around which the large blob of semi-coherent radiation is located. Line 5 is the 1/2 subharmonic of the interval defined by lines 2 and 8. Lines 5 and 6 are the 1/3 subharmonics of lines 4 and 7. (Many lines are multiply defined, as can be seen in this and in the other spectra analyzed.)

5. CHAOS AS A CAUSE OF TRIGGERED EMISSIONS

Since section 4 shows that, in the triggered emission process, sideband radiation is created at the frequencies required by the KAM theorem, we are left with the task of showing why strong spectral lines located at the low frequency end of the spectra are systematically destroyed. Such an explanation can be made with the help of the phase plots in Figure 10.

The results we present are not a consequence of self-consistent calculations. We do not address the issue of sideband growth rates in this paper. We show, instead, a mechanism consistent with the electron equations of motion that indicates why sideband growth and collapse occurs. Such a knowledge is fundamental to suggest, for instance, approximations that will not truncate underlying physical effects when more complete simulations are made.

As mentioned in section 2, the phase plots do not depend directly on Ω_t, but only on the ratio Ω/Ω_t. Ω_t and the particle pitch angle are free parameters, being allowed to take any values we desire. τ is the torque that measures the strength of the inhomogeneity of the magnetic field of the Earth. Its definition is found in III. The plots do not depend directly on τ either, only on the ratio τ/Ω_t^2.

We start with a carrier perturbed by a weak upper-frequency sideband wave located at a frequency Ω, approximately equal to twice the stronger carrier trapping frequency, Ω_t. We assume that the wave amplitude ratio, α, is equal to 0.05 and observe the two-wave interaction at the Earth's equator ($\tau/\Omega_t^2 = 0.0$). Figure 10*a* shows the associated phase plot. We see the weak sideband, its resonance shifted in phase by 180° relative to the main carrier. (This phase choice is made out of convenience. The distortions undergone by the resonances are smaller, and the resulting picture is clearer.) The interaction creates a band of chaos around the main resonance, and a smaller "trapped" resonance near its center.

Figure 10*b* shows the interaction of Figure 10*a* taking place at a point away from the equator, where the inhomogeneity is not zero ($\tau/\Omega_t^2 = 0.02$). We see that the weak sideband resonance has been destroyed by the torque associated with the inhomogeneity (see III), and the chaotic band has been flushed away. However, despite the presence of the weak wave and the effect of the inhomogeneity, the main wave has its resonance mostly intact, capable of producing bunching and wave amplification.

Figure 10*c* shows the effect of sideband growth ($\alpha = 0.2$) on the main wave resonance, at the equator. The main resonance has acquired a "sandy" structure in which electron motion is chaotic. Electrons in such a chaotic region are not capable of being bunched and will not contribute to wave growth. The only remaining regular region is a two-lobed resonance that will radiate away from the main wave, at the frequencies $\pm\Omega/2$ and $\pm\Omega$. As a consequence, sideband growth will completely destroy the ability of the plasma to

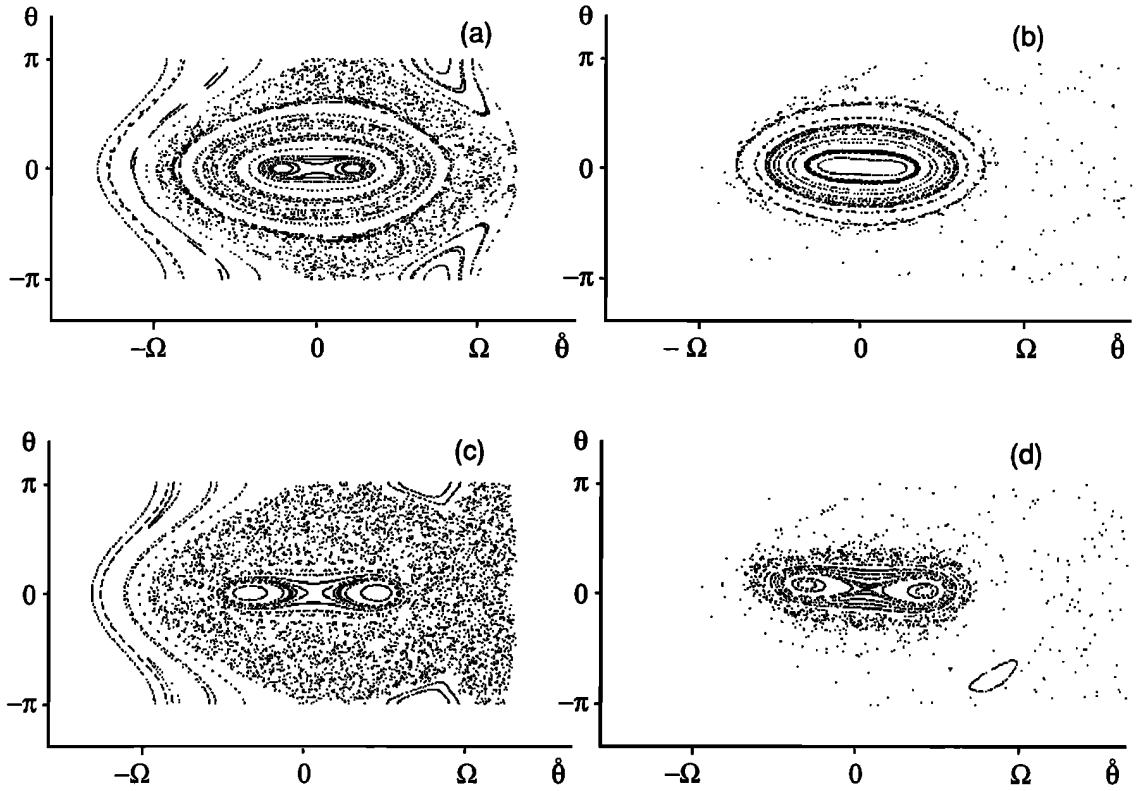

Fig. 10. Simplified representation of a triggered emission. A strong carrier is perturbed by a weak sideband located at a frequency Ω above its own frequency. The sideband wave phase is shifted by 180°: (*a*) $\alpha = 0.05$. $\tau/\Omega_t^2 = 0.0$. The weak sideband resonance is seen. Its presence produces a chaotic band around the main resonance, together with a small "trapped" resonance near its center. Despite the perturbation, the main wave can still be amplified. (*b*) $\alpha = 0.05$. $\tau/\Omega_t^2 = 0.02$. The weak sideband resonance has been destroyed. The chaotic band has been flushed away by the inhomogeneity. The main resonance, however, is not very affected and the main wave can still be amplified. (*c*) $\alpha = 0.2$. $\tau/\Omega_t^2 = 0.0$. The weak sideband resonance is seen. Its growth has completely destroyed the main wave resonance, except for the small "trapped" resonance near its center. The main wave cannot bunch electrons anymore, and it will collapse. (*d*) $\alpha = 0.2$. $\tau/\Omega_t^2 = 0.02$. The chaotic electrons are flushed away by the inhomogeneity, producing an upward burst of electrons that will contribute to the upper sideband growth.

amplify the incoming carrier radiation, and the wave will suddenly collapse back to its input value.

Figure 10*d* shows what happens if in addition to sideband growth we have the inhomogeneity exerting its torque on the electron population ($\tau/\Omega_t^2 = 0.02$). Associated with the wave collapse, there is a sudden burst of electrons flushed upward in frequency. Such an electron burst will behave as a distortion of and an increase in the electron population at higher frequencies, enhancing wave growth in those regions.

In summary, these phase plots represent in a simplified manner all steps observed in the triggered emissions displayed in the data: The transmitted waves grow and shift. They interact among themselves and with PLHs present in the duct, creating sidebands. Sidebands grow, destroying the large wave resonances. The large waves collapse, releasing electrons from their resonances. Those electrons move upwards in frequency (i.e., the electrons have their longitudinal velocities scattered so that they resonate with higher frequency waves), producing a disturbance both in the magnitude and in the gradient of the electron distribution that will enhance sideband growth in the upper side of the frequency spectrum. The process is iterative, leading to the generation of an electromagnetic disturbance that propagates in the time-frequency plane. Such a disturbance is interpreted as a continuous triggered emission (Figures 2–5) when a wide band filter ($\approx$ 10 Hz) analysis is made.

Nunn [1986] presents a mechanism that predicts high growth rates for upper sidebands and low growth rates for lower sidebands, as seen in the data of this paper. He does not address, however, the issue of sideband frequencies or the collapse of sidebands after their growth. The mechanism he presents assumes ordered electron motion and can be treated analytically in a first approximation. It does not involve chaotic phenomena. In this respect it differs from the explanation we presented above that depends strongly on chaotic effects: the upper sidebands are fed by electrons massively scattered in their longitudinal velocity by the overlapping resonances created by the incoming waves. Collectively, this is a diffusion process with diffusion speed controlled by the electromagnetic field. The inhomogeneity defines the direction of diffusion.

6. Discussions and Conclusions

This paper describes data representing triggered emissions that occur when a set of monochromatic waves propagating in a ducted mode in the magnetosphere interact with the hot electron population and, indirectly, with other

types of radiation present in the duct. As has already been observed by *Sá and Helliwell* [1988], "single-frequency" processes do not really exist under those circumstances. Triggered emissions are seen to consist of a complex time-dependent sideband spectrum shifting in frequency with time. Sidebands are created both by the interactions of transmitted waves with one another and with PLR. When only a single carrier is transmitted, sidebands are due exclusively to the interactions between the single carrier and PLHs, indicating that PLR may be essential for the formation of some of the triggered emissions observed and analyzed.

Since triggered emissions are essentially a multi-wave effect, most, if not all of the papers published in the literature on the subject, cannot be entirely adequate for their description. Such papers (see Introduction) consider triggered emissions to be a single wave effect, and have the same shortcomings as the ones that explain "single-frequency" sidebands as coming from the interaction of a single wave interacting with the magnetospheric electrons [e.g., *Nunn*, 1974; *Brinca*, 1972; *Helliwell and Crystal*, 1973].

Nunn [1989] requires a special analysis. He simulates the interaction of a CW pulse with the magnetospheric plasma, obtaining triggered emissions with a layered sideband structure similar to the ones found in the data of this paper. His results, however, do not seem to explain the data consistently. Spectra created by CW pulses must be invariant under small frequency shifts of the transmitted carrier. For a wave transmitted at 4 KHz, shifts of up to ±40 Hz should be permitted if a 1% error in the results is tolerable. The data we present have a frequency structure always explainable by applying the KAM formula to the carrier and PLH frequencies and iterating the results. If one of the spectra simulated by *Nunn* [1989] could be explained in the same way, an arbitrary shift of the transmitted frequency would produce another one that could not. Such shifted spectra, just as valid from a single frequency point of view, have not been observed in either the sideband or triggered emission data.

The reasons for the emphasis on single-wave theories are possible to understand: PLR is weak, not easily detectable in a direct way, and its effects although extremely pronounced are by no means direct or obvious. The negative connotation of the word "PLR" is also an important factor: PLR is considered to be a contamination to be minimized so that the natural phenomena present in the magnetosphere can be adequately studied. Under those circumstances it is not surprising that several authors have embraced the single-carrier hypothesis, and tried to use such a point of view to explain magnetospheric phenomena. On the other hand, from a purely scientific outlook, it is not surprising to find that in a very nonlinear system such as the magnetospheric plasma, a small perturbation of the electromagnetic field is capable of being multiplied and amplified, creating catastrophic effects such as triggered emissions, or less dramatic ones such as the sidebands associated with single-frequency transmissions. (This is an example of the butterfly effect so frequently mentioned in the popular literature about chaotic phenomena.)

Acknowledgments. The author thanks his StarLab colleagues for helpful discussions. He also thanks J. Yarbrough for preparing some of the spectrograms. This work was sponsored by the Division of Polar Programs of the National Science Foundation under grant DPP-86-13783

The Editor thanks D. Nunn and another referee for their assistance in evaluating this paper.

REFERENCES

Brinca, A. L., Whistler side-band growth due to nonlinear wave-particle interaction, *J. Geophys. Res.*, *77*, 3508, 1972.

Carlson, C. R., Simulation and modeling of whistler mode wave growth through cyclotron resonance with energetic electrons in the magnetosphere, Ph.D. Thesis, Stanford Univ., Stanford, Calif., 1987.

Das, A. C., A mechanism for VLF emissions, *J. Geophys. Res.*, *73*, 7457, 1968.

Dowden, R. L., Detrapping by an additional wave of wave-trapped electrons, *J. Geophys. Res.*, *87*, 6237, 1982.

Dowden, R. L., A. D. McKay, L. E. S. Amon, H. C. Koons, and M. H. Dazey, Linear and nonlinear amplification in the magnetosphere during a 6.6 kHz transmission, *J. Geophys. Res.*, *83*, 169, 1978.

Dysthe, K. B., Some studies of triggered whistler emissions, *J. Geophys. Res.*, *76*, 6915, 1971.

Helliwell, R. A., and T. L. Crystal, A feedback model of cyclotron interaction between whistler-mode waves and energetic electrons in the magnetosphere, *J. Geophys. Res.*, *78*, 7357, 1973.

Helliwell, R. A., and U. S. Inan, VLF wave growth and discrete emission triggering in the magnetosphere: A feedback model, *J. Geophys. Res.*, *87*, 3537, 1982.

Molvig, K., G. Hilfer, R. H. Miller, and J. Myczkowski, Self-consistent theory of triggered whistler emissions, *J. Geophys. Res.*, *93*, 5665, 1988.

Nunn, D., A self-consistent theory of triggered VLF emissions, *Planet. Space Sci.*, *22*, 349, 1974.

Nunn, D., A nonlinear theory of sideband stability in ducted whistler mode waves, *Planet. Space Sci.*, *34*, 429, 1986.

Nunn, D., The numerical simulation of VLF nonlinear wave-particle interactions in collision free plasmas using the Vlasov hybrid simulation technique, 42 pp., internal report, Dep. of Electron. and Computer Sci., Southampton Univ., Southampton, 1989.

Paschal, E. W., and R. A. Helliwell, Phase measurements of whistler mode signals from the Siple VLF transmitter, *J. Geophys. Res.*, *89*, 1667, 1984.

Sá, L. A. D., A cyclotron resonance mechanism for very low frequency whistler mode sideband wave radiation, I, Introduction and description of external resonances, *J. Appl. Phys.*, *66*, 3482, 1989*a*.

Sá, L. A. D., A cyclotron resonance mechanism for very low frequency whistler mode sideband wave radiation, II, Description of internal ("trapped") resonances, *J. Appl. Phys.*, *66*, 3495, 1989*b*.

Sá, L. A. D., A cyclotron resonance mechanism for very low frequency whistler mode sideband wave radiation, III, Effect of the inhomogeneity on sideband resonances, *J. Appl. Phys.*, *66*, 3506, 1989*c*.

Sá, L. A. D., and R. A. Helliwell, Structure of VLF whistler mode sideband waves in the magnetosphere, *J. Geophys. Res.*, *93*, 1987, 1988.

Serra, F. M., VLF two-wave-electron interactions in the magnetosphere, *Planet. Space Sci.*, *32*, 985, 1984.

L. A. D. Sá, Space, Telecommunications and Radioscience Laboratory, Stanford University, Stanford, CA 94305.

(Received November 13, 1989;
revised January 29, 1990;
accepted April 10, 1990.)